Evidence for a two-stage particle attachment mechanism for phyllosilicate crystallization in geological processes ⚷

HONGPING HE[1,2,3,*], YIPING YANG[1,2,3], LINYA MA[1,2], XIAOLI SU[1,2], HAIYANG XIAN[1,2], JIANXI ZHU[1,2,3], HUI HENRY TENG[4], AND STEPHEN GUGGENHEIM[5,*]

[1]CAS Key Laboratory of Mineralogy and Metallogeny/Guangdong Provincial Key Laboratory of Mineral Physics and Materials, Guangzhou Institute of Geochemistry, Chinese Academy of Sciences, Guangzhou, 510640, China
[2]CAS Center for Excellence in Deep Earth Science, Guangzhou, 510640, China
[3]University of Chinese Academy of Sciences, Beijing, 100049, China
[4]Institute of Surface-Earth System Science, Tianjin University, Tianjin, 300072, China
[5]Department of Earth and Environmental Sciences, University of Illinois at Chicago, Chicago, Illinois 60607-7059, U.S.A.

ABSTRACT

The understanding of crystal nucleation and growth has evolved over the past two decades from the conventional atom-by-atom model to a non-classical approach, involving particle aggregation and amorphous transformation pathways. Whereas aggregation of particles instead of individual atoms/ions/molecules has been recognized as a common crystallization pathway at the Earth's surface conditions, few cases are known for high-temperature (e.g., melt) mineralization, which is of great importance for understanding geological processes.

Here, we present texture data for natural (e.g., igneous and metamorphic biotite and muscovite) and synthetic (e.g., fluorophlogopite) phyllosilicates suggesting that a particle attachment formation should be considered, although other crystal growth models cannot be excluded. A nonclassical crystallization model is proposed for phyllosilicates forming at elevated temperatures in magmatic and metamorphic environments whereby oriented attachment of building blocks occurs along the (001) plane or the [001] direction, or both simultaneously. In this model, the crystallization of phyllosilicates occurs in steps, with multi-ion complexes forming nanoparticles, and nanoparticles coalescing (self-assembly) to form nano-flakes that become domains in larger crystallites by oriented attachment. Adjacent domains can share a common crystallographic orientation or may be rotated at various angles relative to each other. Nanoparticles may be associated with distorted bonds or may be space separated. Thus, the phyllosilicate grows into a mosaic crystal.

Mosaic crystals can also form following classical crystallization models, but the process differs in that the mosaic character involves the intergrowths of nucleation sites (classical crystal-growth process) instead of the coalescence of nanoparticles building blocks (crystallization by particle attachment). These processes may be discerned by the textural differences that result. Oriented particle attachment of building blocks in phyllosilicates is recognized by a loss of closest packing by bond distortion or by space separation at domain boundaries. Crystallization by atom attachment occurs with closest packing within layers, and particles grow independently. The two processes may occur within a single environment and are not mutually exclusive. However, defects generated, for example, by chemical inhomogeneity, mechanical deformation, or sample preparation, cannot be completely excluded, although the use of synthetic, end-member material (e.g., fluorophlogopite) generated from a melt reduces these possibilities. Nonetheless, a particle attachment model is a viable alternative to classical crystal growth processes for high-temperature phyllosilicates with the presented supporting data, although still not yet proven.

Keywords: Crystal growth, crystallographic orientation, phyllosilicate, building block, nanoparticle

INTRODUCTION

The classic view on crystallization usually involves a nucleation event followed by growth stages proceeding via atom-by-atom addition (Kossel 1927; Stranski 1928; Lee et al. 2001; Liu et al. 2014). Crystal growth may be aided by defects (Frank et al. 1949; Frank 1951; Baronnet 1975; Sunagawa and Koshino 1975) that lead to the formation of kinks and subsequently facilitate the attachment of atoms or ions. Screw dislocations are particularly important for this growth mechanism because the resultant growth spiral enhances crystallization by providing a continuous supply of steps and kinks and at the same

time limits new nucleation as ions more readily attach to kink sites than self-organize into two-dimensional nuclei under most circumstances. Based primarily on microscopic texture data, two basic crystal growth models, layer-by-layer growth (i.e., Kossl-Stranski two-dimensional nucleation growth) and spiral growth (i.e., BCF theory) were proposed in the mid-1900s, which successfully described observations of crystal growth that were available at that time.

However, a growing body of observations on field and laboratory samples shows that crystals can form by the attachment of particles ranging from multi-ion complexes to fully formed nanoparticles (De Yoreo et al. 2015; Lee et al. 2016). In this nonclassical model, oriented attachment (OA) is proposed to be a key step by which aggregating nanoparticles self-assemble into extended structures by preferential attachment on specific crystal faces. Crystallization by particle attachment (CPA) occurs for various minerals, such as apatite (Habraken et al. 2013), anatase (Penn and Banfield 1998b), iron oxyhydroxides (Banfield et al. 2000), magnetite (Baumgartner et al. 2013), zeolites (Lupulescu and Rimer 2014), and many others. Particle-based mineral formation may have particular importance for geochemical cycling of elements and the transition from an inorganic to a biological world, as well as synthesis of novel nanomaterials (De Yoreo et al. 2015).

Nearly all the reported minerals involving such nonclassical pathways are three-dimensional (3D) crystals formed at the Earth's surface conditions (mostly associated with biomineralization) (Banfield et al. 2000; Oaki and Imai 2005; Gong et al. 2012) or hydrothermally synthesized in the laboratory (Penn and Banfield 1998a, 1999; Baumgartner et al. 2013; Smeets et al. 2017), while little consideration has yet been given to higher temperature (e.g., melt) environments. Knowledge of high-temperature crystallization is of great importance for a comprehensive understanding of mineral crystallization and consequently for obtaining critical information related to igneous and metamorphic processes. Hence, the main objective of this study is to determine the crystal growth mechanism of phyllosilicate minerals at elevated temperatures by considering natural and synthetic micas. Our results indicate that nanoparticles, which form at an early stage of crystallization, form the basic building blocks of coarsening phyllosilicate crystals. Phyllosilicate crystallization occurs mainly by the initial formation of multi-ion clusters (nucleation), which form precursory nanoparticles that self-assemble to form nano-flakes, which then become domains in larger crystallites by oriented attachment. This study not only describes a novel crystallization pathway for phyllosilicates, but also suggests that the microstructure of phyllosilicate crystals may in part indicate the evolution of melts and other geological fluids involved in geochemical processes.

MATERIALS AND METHODS

Natural biotite and muscovite samples

Two groups of natural mica samples of magmatic and metamorphic origin were investigated. A magmatic muscovite from a granitic pegmatite and a biotite from a biotite granite were collected from Zhaoqing, Guangdong Province, China (Yang et al. 2020). A metamorphic muscovite and a metamorphic biotite were collected from Shijiazhuang, Hebei Province, China. More specifically, the muscovite was from the Lingshou-Baishan sedimentary-metamorphism-type mica deposit, hosted by muscovite K-rich feldspar gneiss, whereas the biotite occurred

in a biotite plagioclase gneiss.

X-ray diffraction (XRD) patterns indicate that the samples investigated are pure biotite or muscovite (see details in Online Material[1] Figs. OM1–OM2), with the XRD measurements conducted on a Bruker D8 Advance diffractometer with Cu$K\alpha$ radiation (He et al. 2014). The major elemental components of the mica samples were determined by using a JEOL JXA-8230 electron probe micro-analyzer (EPMA), following the procedure described by Tan et al. (2016). On the basis of EPMA results (see details in Online Material[1] Tables OM1–OM4), their calculated chemical formulas are as follows:

Magmatic biotite: $(K_{0.930}Na_{0.012}Ca_{0.001})_{\Sigma0.943}(Ti_{0.125}Mn_{0.036}Fe_{1.387}Mg_{0.901}$
$Mn_{0.036}\square_{0.515})_{\Sigma3}(Si_{2.533}Al_{1.414}Fe_{0.053})_{\Sigma4}O_{10}(OH,F)_2$

Magmatic muscovite: $(K_{0.889}Na_{0.060})_{\Sigma0.949}(Al_{1.811}Mg_{0.049}Ti_{0.015}Fe_{0.095}Mn_{0.028})_{\Sigma1.998}$
$(Al_{0.881}Si_{3.119})_{\Sigma4}O_{10}(OH)_2$

Metamorphic biotite: $(K_{0.883}Na_{0.029})_{\Sigma0.912}(Al_{0.320}Ti_{0.145}Fe_{0.853}Mg_{1.512}Mn_{0.007}\square_{0.163})_{\Sigma3}$
$(Si_{2.796}Al_{1.204})_{\Sigma4}O_{10}(OH,F)_2$

Metamorphic muscovite: $(K_{0.900}Na_{0.057})_{\Sigma0.957}(Al_{1.742}Mg_{0.065}Ti_{0.031}Fe_{0.231})_{\Sigma2.069}$
$(Al_{0.900}Si_{3.100})_{\Sigma4}O_{10}(OH)_2$

Synthetic fluorophlogopite

To test the crystal growth mechanism indicated by the natural mica samples, two fluorophlogopite samples of high purity (Online Material[1] Fig. OM3) were synthesized at 900 and 1450 °C, respectively, and their microstructures were investigated. All the chemicals used for the synthesis of fluorophlogopite were of analytical grade, including amorphous SiO_2 purchased from Aladdin Industrial Corporation, K_2SiF_6 and $MgCl_2$ from Fuchen Chemical Factory, and Al_2O_3, MgO, NaF, and $Na_2SiO_3·9H_2O$ from Guangzhou Chemical Factory. Kaolinite with a purity of more than 96%, serving as a coupling agent and starting material in the synthesis experiments, was collected from Maoming, Guangdong Province, China.

Synthesis of fluorophlogopite at 1450 °C. The mixture composed of SiO_2 (30.7 wt%), Al_2O_3 (11.6 wt%), MgO (32.6 wt%), and K_2SiF_6 (25.1 wt%) was well ground in an agate mortar for 30 min and then transferred to a 50 mL corundum crucible. A coupling agent was prepared with kaolinite and $Na_2SiO_3·9H_2O$ in a mass ratio of 1:1, which was pasted on the inner surface of the crucible to reduce the loss of fluorine. The crucible was placed into a muffle furnace and was heated to 1450 °C at a heating rate 10 °C/min. After being maintained for 4 h at this temperature, which produced a melt, the furnace was freely cooled to room temperature.

Synthesis of fluorophlogopite at 900 °C. Kaolinite (40.0 wt%), NaF (20.0 wt%), and $MgCl_2$ (40.0 wt%) were mixed and transferred to a 50 mL corundum crucible and heated in a muffle furnace at 900 °C for 5 h, and then freely cooled to room temperature. The obtained product was washed with deionized water three times and then dried at 60 °C for 12 h. Both the phase identifications and composition determinations (see details in Online Material[1] Fig. OM3 and Tables OM5–OM6) were conducted similarly following the procedures described for the natural mica samples. Their calculated chemical formulas are as follows:

Fluorophlogopite synthesized at 900 °C:
$(K_{1.00}Na_{0.012})_{\Sigma1.012}(Mg_{2.811}Al_{0.160})_{\Sigma2.971}(Si_{2.882}Al_{1.118})_{\Sigma4}O_{10}F_{2.00}$

Fluorophlogopite synthesized at 1450 °C:
$(K_{0.970}Na_{0.011})_{\Sigma0.981}(Mg_{2.672}Al_{0.271})_{\Sigma2.943}(Si_{2.768}Al_{1.232})_{\Sigma4}O_{10}F_{2.00}$

High-resolution transmission electron microscopy (HRTEM)

To investigate stacking structures of phyllosilicates along the [001] direction, oriented samples were embedded in epoxy resin and dried at 100 °C for 3 h. Subsequently, ultrathin sections with a thickness of ~75 nm were sliced with a diamond knife using a Lecia EM UC7 ultramicrotome. The sections were placed on carbon-coated copper micro-grids for TEM and high-angle annular dark-field scanning transmission electron microscopy (HAADF-STEM) with an FEI Talos F200S microscope at an accelerating voltage of 200 kV.

RESULTS AND DISCUSSION

Magmatic biotite and muscovite

Scanning transmission electron microscope (STEM) images of granitic biotite (Fig. 1a) clearly show that the particle (projection down the [010] direction) with a size of ~140 × 120 nm is comprised of at least 5 domains (i.e., nano-flakes) stacking along
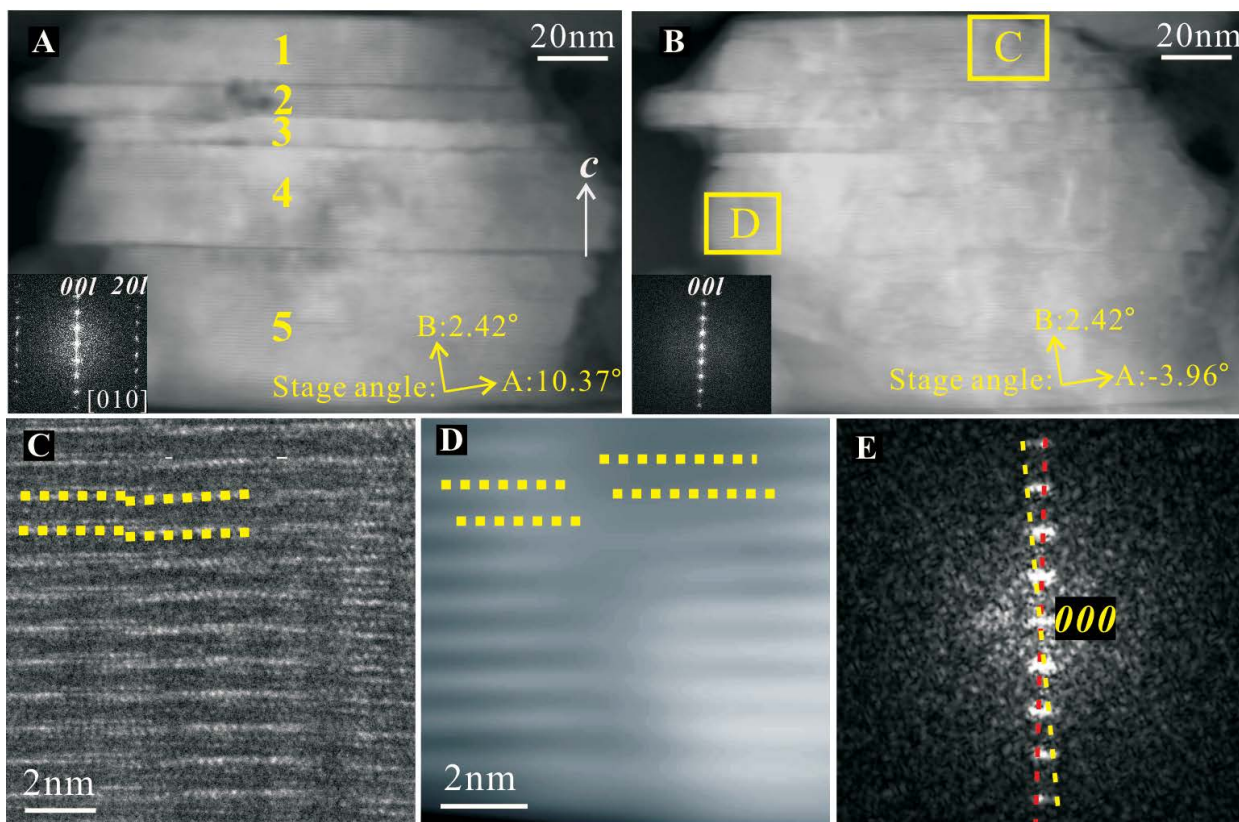
FIGURE 1. STEM/HRTEM images and FFT patterns of biotite from a granite at different stage angles. The two STEM images (**a** and **b**) correspond to the [010] zone axis (**a**) and an arbaitrary axis [*hkl*] (**b**), respectively. The domains in **b** are composed of nanoparticles, which are linked by bond distortions or separated by space (**c** and **d**). The dotted lines correspond to biotite layers. (**e**) Two series of diffraction lines in the FFT pattern obtained from the zone of **c**, implying slightly different orientations of the component nanoparticles.

the *c* axis (as numbered in Fig. 1a). The thickness of these domains varies from ~7 to ~40 nm. The interface between domains is distinguished by differing contrasts and a "zigzag" profile at the edge of the particle.

After a ~14.3° rotation of the biotite particle in Figure 1a, the ultra-fine structure showed distortions and separated space between adjacent nanoparticles (Fig. 1b). The HAADF-STEM images demonstrate that the domains are comprised of nanoparticles with layer distortion (Fig. 1c) or separated space (Fig. 1d) at the boundaries between two adjacent nanoparticles. The corresponding fast Fourier transform (FFT) pattern (Fig. 1e) shows two series of independent diffraction patterns, indicating a small difference in crystallographic orientation between the two nanoparticles connected by layer distortion. When structurally similar edges of biotite nanoparticles approach, there is a driving force to form chemical bonds between atoms of opposing edges to achieve full coordination. Because edges are not atomically flat, coherence is achieved by distortion at the interface (Penn and Banfield 1998a). Some nanoparticles are partially connected by continuous layers, whereas others are spatially separated (Fig. 1d), suggesting an intermediate or alternative state for oriented attachment of initial nanoparticles (Li et al. 1999).

Although the FFT image shows that most nanoparticles in the biotite grain share the same crystallographic orientation, i.e., the

[010] direction (Fig. 1a, inset), random rotations between two adjacent nano-flake domains were also found. Figure 2 shows a rotation of ~5° between the two adjacent domains; the projection of the upper domain is along the [110] zone axis (Fig. 2b), whereas the lower domain only displays (00*l*) diffractions (Fig. 2c). Also, a screw dislocation was observed in the lower domain (Fig. 2a, bottom). This may suggest that a spiral growth mechanism is involved in the formation of initial nanoparticles, which is rarely reported in 3D crystals formed via crystallization by particle attachment (Penn and Banfield 1998a).

Our observations indicate that magmatic biotite has a hierarchical fine structure, with grains comprised of domains that are composed of aggregated nanoparticles. Both layer-by-layer growth and spiral growth are involved in the formation of nanoparticles during melt cooling, whereas coarsening of crystals is controlled by oriented attachment of formed domains. Such a crystal growth pathway is different from the traditional crystal growth mechanisms for rock-forming minerals (Kossel 1927; Stranski 1928; Frank et al. 1949; Frank 1951), and the nonclassical pathways observed in biomineralization products and hydrothermally synthesized minerals (De Yoreo et al. 2015; Lee et al. 2016).

Similar nanoparticle aggregates are also found in magmatic muscovite grains (Figs. 3a and 3b) collected from a granitic
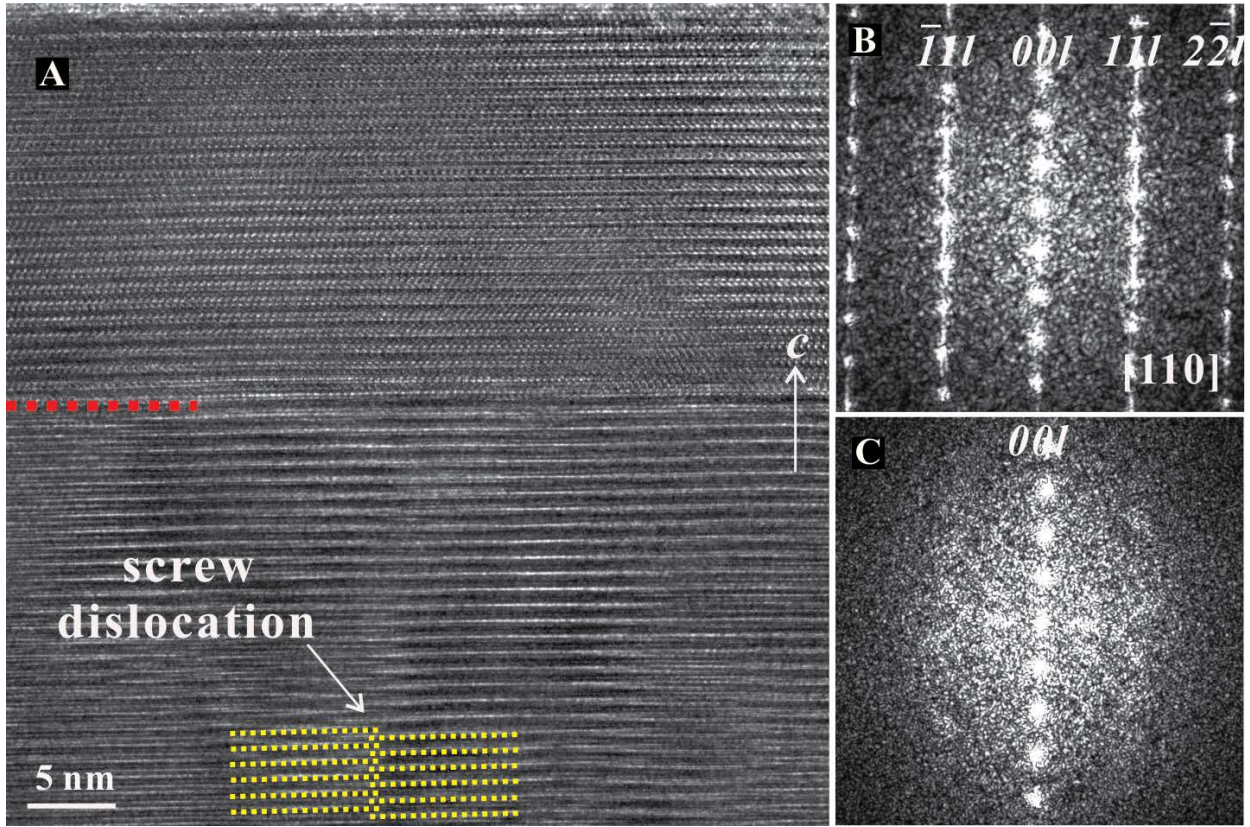
FIGURE 2. HRTEM image and FFT patterns of biotite from a granite. HRTEM image of two biotite grains (**a**) and FFT patterns of the corresponding domains show that the upper domain is along the [110] zone axis (**b**) and the lower one only displays (00*l*) diffraction spots (**c**). A screw dislocation is observed in the lower domain. The dotted lines represent biotite layers.
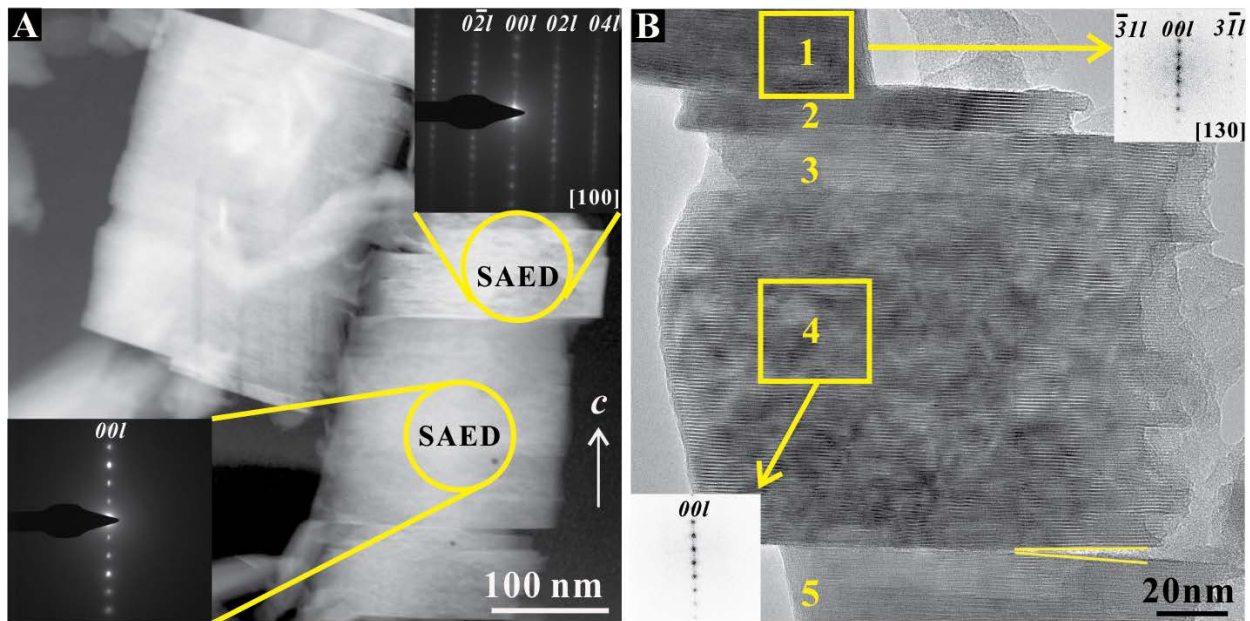

FIGURE 3. STEM/HRTEM images and SAED/FFT patterns of muscovite from a pegmatite. (**a**), STEM image of muscovite grain. The SAED patterns (insets in **a**) show that the crystallographic orientations of the domains within a grain are different from each other. (**b**) The muscovite grain is comprised of 5 nano-flakes with random rotations.

pegmatite. Compared with biotite, the orientations of domains within a single muscovite grain usually differ from one another to a larger extent based on the selected-area electron diffraction (SAED) patterns. For instance, the STEM image of the upper domain (marked with the circle in yellow) is along the [100] zone axis, whereas the lower domain only displays (00*l*) diffractions (Fig. 3a, insets), corresponding to a rotation of ~11° relative to each other. As shown in Figure 3b, the muscovite grain is comprised of five domains with random rotations via oriented attachment along the *c* axis. Such an orientation difference may result from variations between the crystallization environments (e.g., temperature, viscosity, activity of H_2O, etc.) of biotite (granite) and muscovite (pegmatite).

Metamorphic biotite and muscovite

HRTEM observations of metamorphic biotite and muscovite crystals show that despite both minerals being composed of domains involving nano-flakes, the observed rotational offset of the domains varied widely between them. The rotation angles are very different from one to another and not related to polytype formation of n ×60° (0 ≤ n ≤ 5) (Smith and Yoder 1956; Ross et al.

1966; Baronnet 1972). As shown in Figure 4a, the metamorphic biotite grain is comprised of three domains, where the crystallographic orientations of domains 1 and 2 are similar (a relative rotation of ~1–2°), whereas those of domains 2 and 3 involve a rotation of ~7° relative to each other. Such a mismatch results in the formation of edge dislocations (the arrow in Fig. 4b), which is similar to those that result from the imperfect oriented attachment of synthetic anatase (Penn and Banfield 1998a).

The metamorphic muscovite grain in Figure 5a is composed of at least five nano-flake domains. The enlarged image of the area (see yellow square) shows that the layer stacking at the interface between the two domains is continuous along the [001] direction (Fig. 5b). However, the FFT patterns indicate that domain 1 is along the [110] zone axis (Fig. 5c), whereas domain 2 is along the [010] zone axis (Fig. 5d), indicating a rotation of ~30° (or ~150°) between domains 1 and 2. The angular mismatch between adjacent domains is ubiquitous within metamorphic biotite and muscovite as can be observed in other randomly selected observation areas (Online Material[1] Figs. OM4–OM5).

In domain 2 (Fig. 5b), there are angular differences between the FFT patterns of three areas, i.e., a regular stacking region
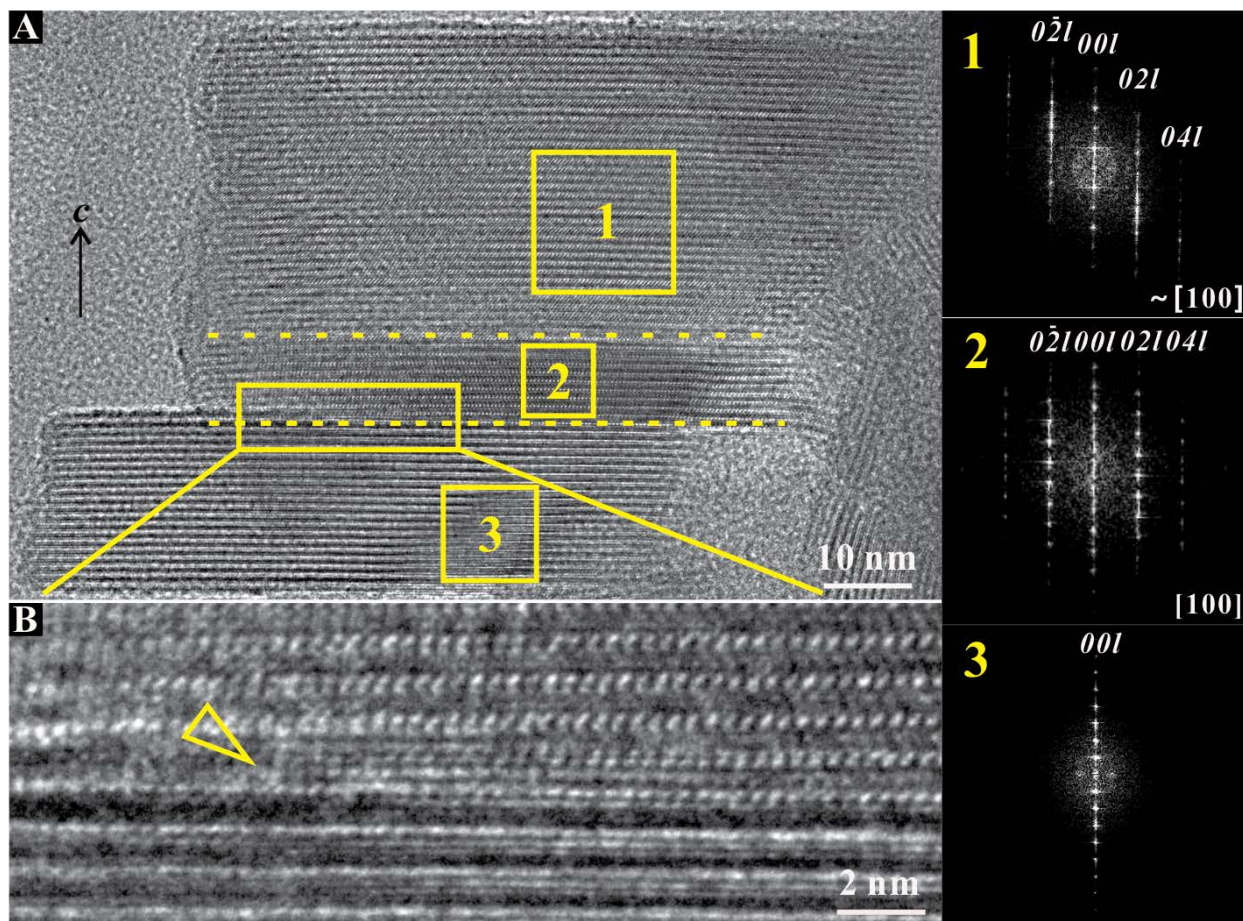

FIGURE 4. HRTEM images of metamorphic biotite. (**a**) Three attached biotite domains with rotation about the *c* axis. Dashed lines represent the interfaces between domains. (**b**) The enlarged image of the yellow square in **a**, which displays an edge dislocation (arrowhead) at the interface. The right side displays FFT patterns of biotite nano-flakes in **a**. Similar orientation for domains 1 and 2 but a rotation of ~7° for domain 3 relative to domains 1 and 2.

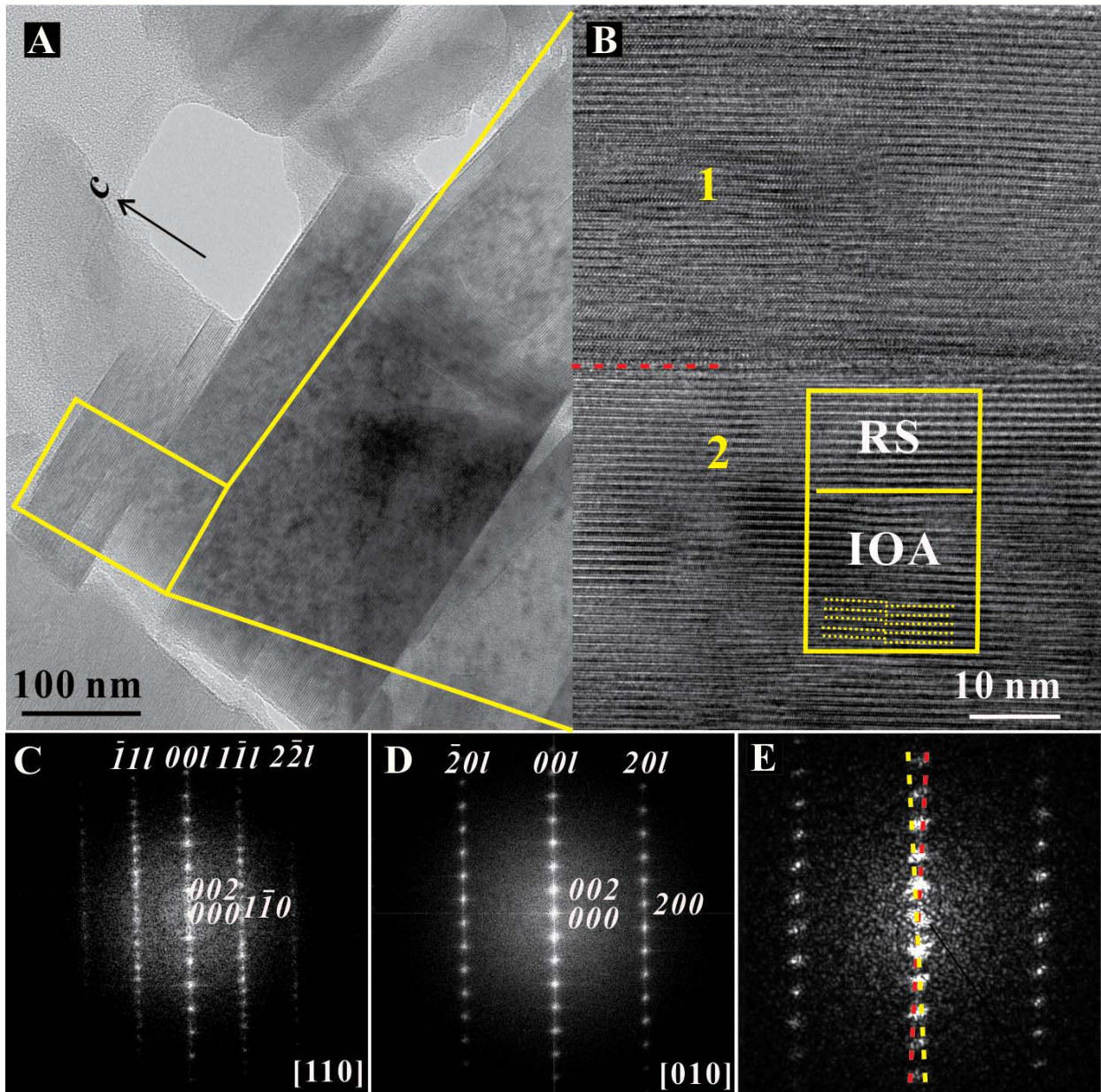**FIGURE 5.** HRTEM images and FFT patterns of metamorphic muscovite. (**a**) Muscovite domains of nano-flakes along the *c* axis. (**b**) The enlarged image of the yellow square in **a**. RS = regular stacking; IOA = imperfect oriented attachment. The dotted lines in the IOA region represent muscovite layers. (**c–d**) FFT patterns of domain 1 and 2 in **b**, respectively. (**e**) FFT pattern of the IOA region in **b** shows at least two series of independent diffraction lines.

(box labeled "RS"), an imperfect oriented attachment region (box labeled "IOA"), and an unlabeled area to the left of "10 nm." The tilt angle of the imperfect oriented attachment region is much smaller than that of the unlabeled region. Following Penn and Banfield (1998a), both regions possibly result from oriented attachment, but other factors (e.g., chemical heterogeneity) indicated by the variations in HAADF-STEM intensity (Fig. 5b) also cannot be excluded. The region of regular stacking and the region of imperfect oriented attachment are joined by regular stacking, suggesting a nucleation and growth process, although the dislo-

cation within the latter was generated by an imperfect oriented attachment. As observed in FFT patterns (Fig. 5e), multiple series of independent diffraction points are recognized, which shows both oriented attachment and nucleation and growth processes.

Random rotation of component domains occurs extensively in metamorphic biotite and muscovite grains, whereas in magmatic micas those domains usually share a common crystallographic orientation, suggesting mica can form by oriented attachment of nano-flakes/nanoparticles. However, the ultra-fine structure of mica closely correlates with the environments in which they

form. Presumably, the temperature, cooling rate, and other environmental conditions may be dominant factors controlling the microstructure of mica crystals. High temperature and low cooling rate are favorable conditions for the formation of homogeneous phyllosilicate crystals. Otherwise, the crystals are heterogeneous, in accord with thermodynamic and kinetic crystal growth theories (ten Wolde and Frenkel 1997).

Synthetic fluorophlogopite

To test the afore-discussed growth mechanism, we synthesized fluorophlogopite (analogous to natural mica from melts) from the molten state and examined the fine structure of the product. The harvested crystals are transparent and colorless crystalline lamellae several micrometers to millimeters in size (Chen et al. 2019). The TEM images and SAED patterns show that the synthetic fluorophlogopite grains are formed by stacking of domains with different crystallographic orientations along the c axis (Online Material[1] Fig. OM6). Similar to the aforementioned natural micas, the HRTEM images on crystalline (lattice-fringe-bearing) regions with low contrast show that the synthetic fluorophlogopite domains are also comprised of nanoparticles connected by nearly continuous layers between adjacent nanoparticles (Figs. 6a and 6b). The FFT pattern displays separated and strong diffraction points (Fig. 6a, inset). The continuity of lattice fringes and separated diffraction points demonstrate that all domains have the same crystallographic orientation (a defective single crystal). Figure 6b shows that these nanoparticle domains prefer to attach to each other along (010), (110), and ($\bar{1}$10) faces, which are stable edge surfaces according to the stable-bond-chain theory (White and Zelazny 1988). These stable edge surfaces are formed during the nucleation of nanoparticles at the onset of crystallization. Oriented attachment of these nanoparticles then leads to the formation of nano-flakes, which become the basic

building blocks of the synthetic phyllosilicate grains.

Although most of the synthetic fluorophlogopite crystals are near perfect, the relative rotations of their constituent nanoparticles and nano-flakes are observed in the HRTEM results (Fig. 7). The fluorophlogopite grain is comprised of 10 nano-flakes (Fig. 7a). Nano-flakes 1–4 (projection down the [130] direction) and nano-flakes 5–10 (projection down the [110] direction) share a common crystallographic orientation, respectively, whereas a ~20° rotation occurs between nano-flakes 1–4 and nano-flakes 5–10. A similar rotation angle was also observed between adjacent nano-flakes on another randomly selected fluorophlogopite grain (Fig. 7b). The projection of the upper domain is along the [110] zone axis, whereas that of the lower one is along the [130] zone axis, i.e., a ~20° rotation between the two domains.

As shown in Figure 8a, the fluorophlogopite grain is comprised of 7 nano-flakes with distinct boundaries, in which a dislocation line occurs at the right edge of domain 6 (Fig. 8b). In addition, the orientation of the area marked by the yellow square (as indicated by the corresponding FFT pattern at the left in Fig. 8c) is different from that of the other part of this nano-flake (see the FFT pattern at the right), suggesting the nano-flake is formed by the imperfect oriented attachment of nanoparticles.

Phyllosilicate crystal growth mechanism

Mica minerals (e.g., biotite and muscovite) are common in geologic environments. In the traditional model, the mica structure is characterized by identical or near identical layers that stack along the c axis (Smith and Yoder 1956; Ross et al. 1966; Baronnet 1972; Bailey 1984; Brigatti and Guggenheim 2002), with a large interlayer cation (e.g., K$^+$) between adjacent layers. In the process of crystal growth, rotation of mica layers with regular angles (i.e., n ×60°, 0 ≤ n ≤ 5) may occur and leads to polytypism (Smith and Yoder 1956; Ross et al. 1966; Baronnet
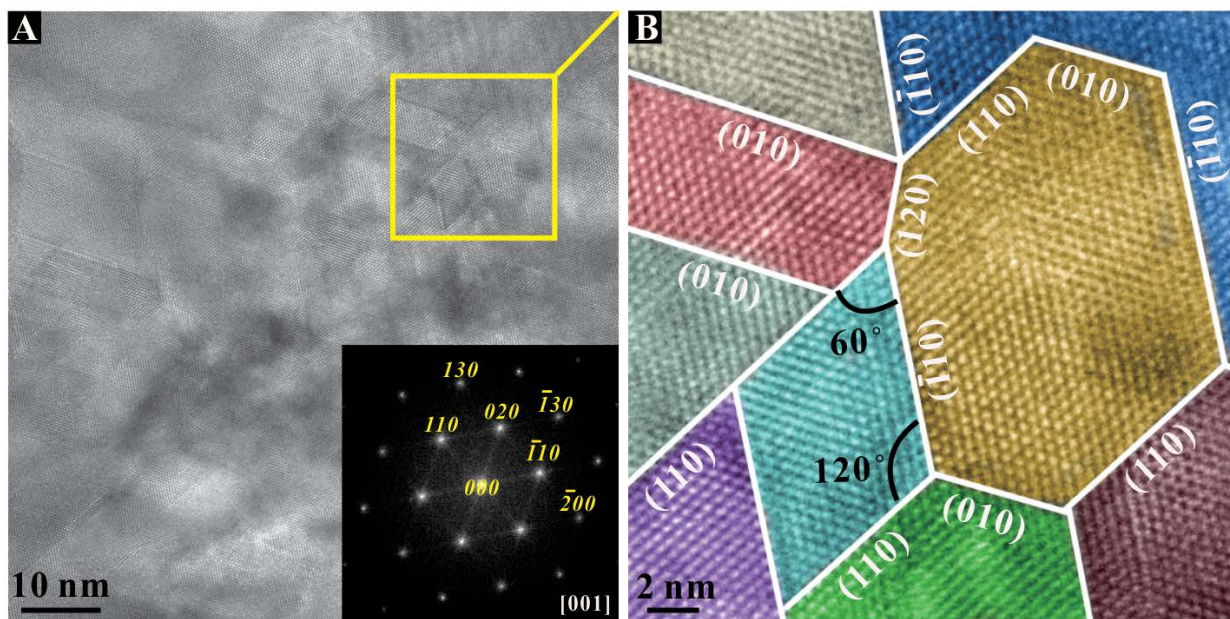

FIGURE 6. HRTEM images of synthetic fluorophlogopite from a melt. (**a**) Synthetic fluorophlogopite (synthesized at 900 °C) is comprised of domains of nanoparticles with parallel crystallographic orientation, as indicated by FFT pattern (inset). (**b**) The enlarged image of the area marked with square in **a**, displaying oriented attachment between different nanoparticles (domains).
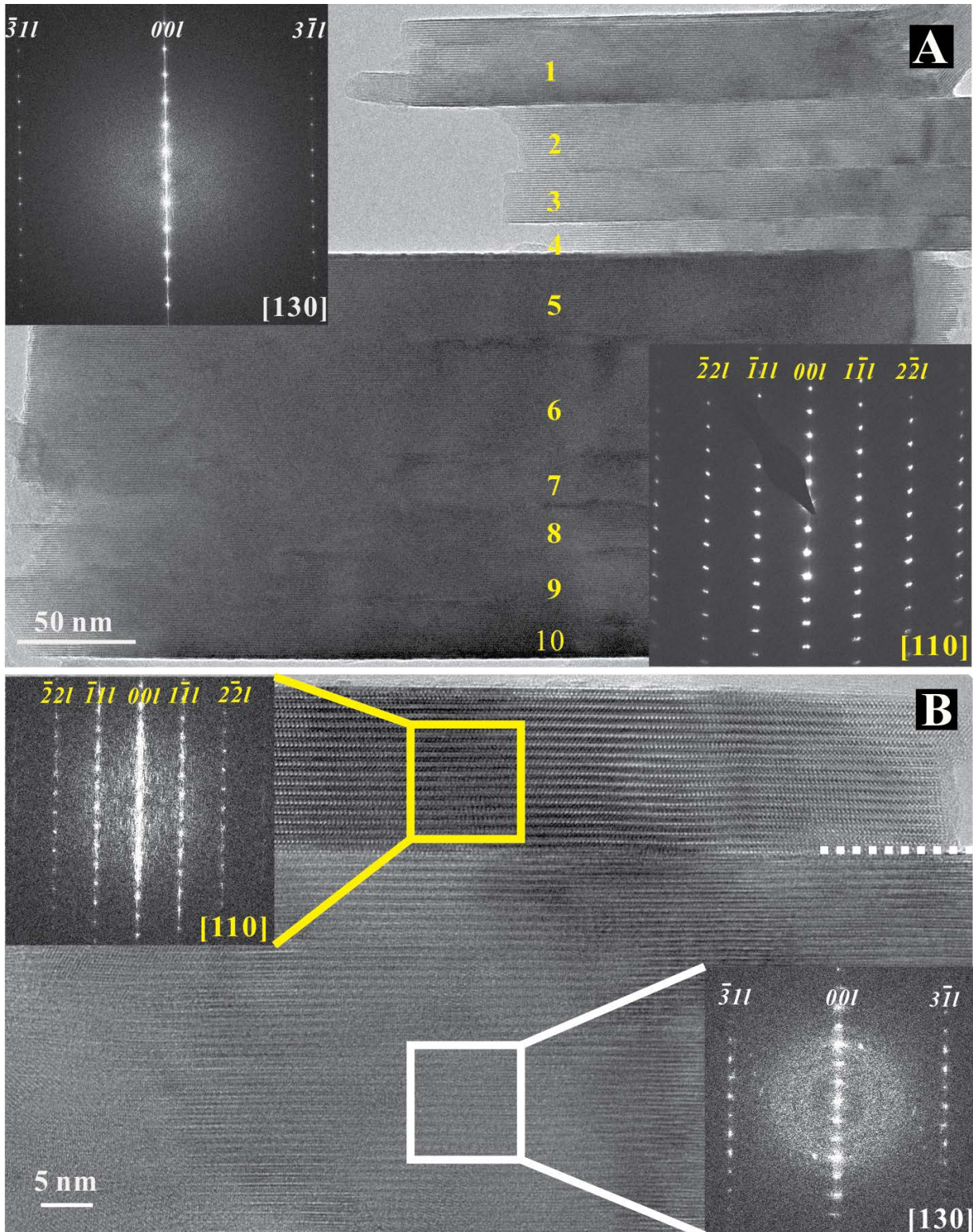
Figure 7. TEM/HRTEM images and SAED/FFT patterns of the fluorophlogopite synthesized at 1450 °C. (**a**) TEM image and SAED/FFT patterns (insets) of the synthetic fluorophlogopite. FFT pattern (upper lift) was taken from nano-flakes 1–4 (projection down the [130] direction), and SAED pattern (lower right) from nanoflakes 5–10 (projection down the [110] direction), respectively. (**b**) HRTEM image and FFT patterns (insets) of the synthetic fluorophlogopite. The dotted line in **b** showing the grain boundary of the two domains. Note that **a** and **b** were obtained from different fluorophlogopite grains.
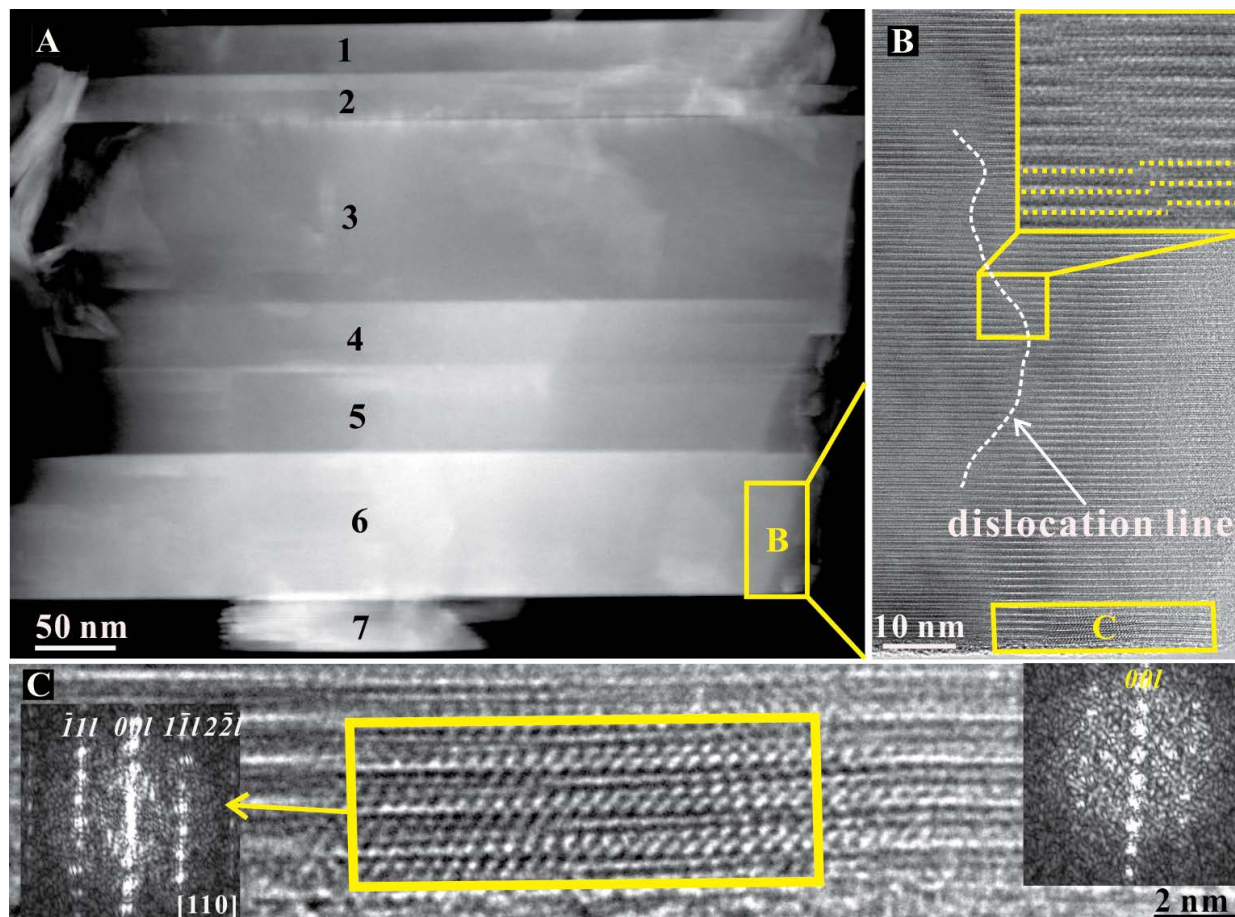
Figure 8. STEM/HRTEM images and FFT patterns of the fluorophlogopite synthesized at 1450 °C. (**a**) STEM image of the synthetic fluorophlogopite. (**b**) HRTEM image enlarged from the marked area of nanoflake 6 in **a**. The inset (upper right) is the enlarged image of the yellow square (around the midpoint) to show the dislocation line observed. The dotted lines in the inset represent the fluorophlogopite layers. (**c**) HRTEM image and the corresponding FFT patterns of the synthetic fluorophlogopite marked by the yellow rectangle at the bottom of **b**.

1972), and ion attachment proceeds via a spiral growth mechanism along screw dislocations (Baronnet 1975; Sunagawa 2007). Thus, atom-by-atom addition and layer-by-layer stacking have been suggested to be the growth mechanism for mica minerals.

However, the results acquired here on natural and synthetic micas suggest that nanoparticles are involved in the mineralization of phyllosilicates under geological conditions. The crystallization is believed to occurs as in a two-stage process after multi-ion complexes form: (1) the formation of nanoparticles and the ensuing oriented particle aggregation in which the building blocks may share a common crystallographic orientation or may have a small rotation relative to each other in route to the formation of phyllosilicate nano-flakes; and (2) the coarsening of grains via attachment of the nano-flakes in which the orientation of individual nano-flakes can vary randomly. In this process, the product of each step becomes the building unit for the next. Whereas the oriented attachment occurs primarily in the (001) plane, coarsening is responsible for the Z-direction growth (extension in the [001] direction) (Fig. 9). The two-stage process appears to be favored by a high energy state as indicated by better flake continuity at high temperature, whereas directed

stress may play a role to enhance the oriented attachment of nanoparticles during metamorphism.

As shown by previous studies (Lee Penn et al. 2007; De Yoreo et al. 2015) in lower temperature environments, the nanoparticles in oriented aggregates are usually several nanometers in diameter, and sometimes, adjacent nanoparticles are space separated. However, nanoparticles from melts and other high-temperature systems, as demonstrated by the present study, are much larger (about several tens or hundreds of nanometers), and the resultant particles display some structural continuity. The larger size and structural continuity may result from the difference between melt and solution hosted crystallization (Nanev 2015). For crystal coarsening via particle attachment, driving forces are critical for particle movement and collision (Gibbs et al. 2011; Wallace et al. 2013; Zhang et al. 2014) as well as orientation adjustment between adjacent nanoparticles (Penn and Banfield 1998a). In the case of a solution, due to a relatively low temperature, nanoparticle movement is relatively slow and orientation adjustment is commonly difficult, resulting in a low crystal growth rate and imperfect crystal structure. However, in the case of a melt, Brownian motion-driven particle collisions
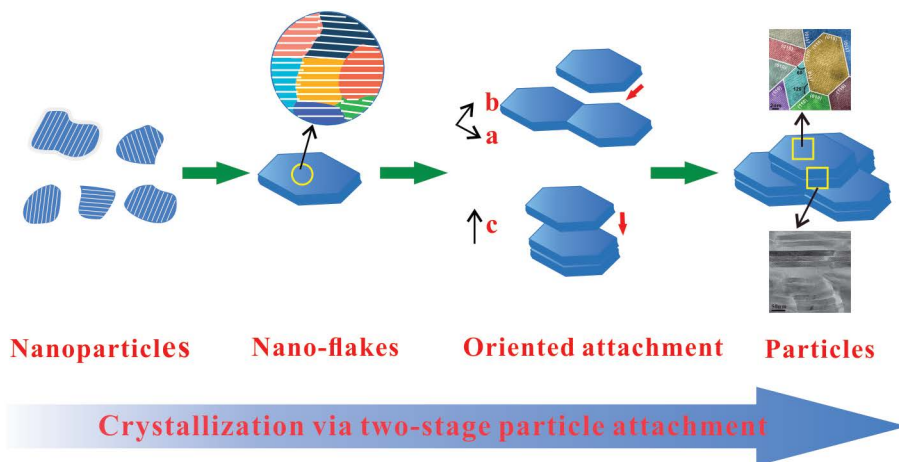
FIGURE 9. Schematic showing crystallization from nanoparticles to particles. Multi-ion complexes are precursory to nanoparticles and are not depicted in the diagram. After nano-flakes are formed from nanoparticles and incorporated into the particle by oriented attachment, they are referred to as domains (or domains of nano-flakes) in the text.

and orientation adjustments are feasible, leading to the formation of crystals with larger size and component nanoparticles sharing a common crystallographic orientation.

IMPLICATIONS

The present study indicates that, whereas crystallization by particle attachment is widely observed for aqueous phase crystallization, oriented attachments are also likely to occur in melts, high-temperature fluids, and high-grade metamorphic regimes. Due to their unique two-dimensional crystal structures, we speculate that the two-stage attachment may be a possible growth mode in the high-temperature state for phyllosilicates.

More importantly, this study suggests that the size of the nanoparticles and the microstructure of the resultant aggregations (e.g., boundary state and extent of bond distortion) strongly depend on the local environments involved. Thus, for mineral crystallization from magmas and high-temperature metamorphic processes, the size and relative orientation of the nanoparticles may be used as indicators for a fine-scale understanding of the evolution of the melts and high-grade metamorphic fluids and for constraining the concurring physicochemical conditions. For instance, a larger nanoparticle size in resultant mineral crystals suggests a slower cooling rate within the melt. The relationship between the features of mineral crystals (e.g., nanoparticle size) and the evolution of melts (e.g., cooling rate) can further the understanding of geological processes.

REFERENCES CITED

Bailey, S.W. (1984) Classification and structures of the micas. Reviews in Mineralogy and Geochemistry, 13, 1–12.
Banfield, J.F., Welch, S.A., Zhang, H., Ebert, T.T., and Penn, R.L. (2000) Aggregation-based crystal growth and microstructure development in natural iron oxyhydroxide biomineralization products. Science, 289, 751–754.
Baronnet, A. (1972) Growth mechanisms and polytypism in synthetic hydroxylbearing phlogopite. American Mineralogist, 57, 272–1293.
——— (1975) Growth spirals and complex polytypism in micas. I. Polytypic structure generation, Acta Crystallographica, A31, 345–355.
Baumgartner, J., Dey, A., Bomans, P.H.H., Coadou, C.L., Fratzl, P., Sommerdijk, N.A.J.M., and Faivre, D. (2013) Nucleation and growth of magnetite from solution. Nature Materials, 12, 310–314.
Brigatti, M.F., and Guggenheim, S. (2002) Mica crystal chemistry and the influence of pressure, temperature, and solid solution on atomistic models. Reviews in Mineralogy and Geochemistry, 46, 1–97.
Chen, A., Tan, W., He, H., Li, G., Wu, X., Tao, Q., and Zhu, J. (2019) Chemical and structural studies of coexisting $1M$-and $2M_1$-polytypes in synthetic fluorophlogopites and influence of Al on the polytype formation. Physics and Chemistry of Minerals, 46, 259–270.
De Yoreo, J.J., Gilbert, P.U.P.A., Sommerdijk, N.A.J.M., Penn, R.L., Whitelam, S., Joester, D., Zhang, H.Z., Rimer, J.D., Navrotsky, A., Banfield, J.F., and others (2015) Crystallization by particle attachment in synthetic, biogenic, and geologic environments. Science, 349, aaa6760.
Frank, F.C. (1951) CII. The growth of carborundum: Dislocations and polytypism. The London, Edinburgh, and Dublin Philosophical Magazine and Journal of Science, 1014–1021.
Frank, F.C., van der Merwe, J.H., and Mott, N.F. (1949) One-dimensional dislocations. I. Static theory. Proceedings of the Royal Society of London. Series A. Mathematical and Physical Sciences, 198, 205–216.
Gibbs, G.V., Crawford, T.D., Wallace, A.F., Cox, D.F., Parrish, R.M., Hohenstein, E.G., and Sherrill, C.D. (2011) Role of long-range intermolecular forces in the formation of inorganic nanoparticle clusters. The Journal of Physical Chemistry A, 115, 12933–12940.
Gong, Y.U.T., Killian, C.E., Olson, I.C., Appathurai, N.P., Amasino, A.L., Martin, M.C., Holt, L.J., Wilt, F.H., and Gilbert, P.U.P.A. (2012) Phase transitions in biogenic amorphous calcium carbonate. Proceedings of the National Academy of Sciences, 109, 6088–6093.
Habraken, W.J.E.M., Tao, J.H., Brylka, L.J., Friedrich, H., Bertinetti, L., Schenk, A.S., Verch, A., Dmitrovic, V., Bomans, P.H.H., Frederik, P.M., and others (2013) Ion-association complexes unite classical and non-classical theories for the biomimetic nucleation of calcium phosphate. Nature Communications, 4, 1–12.
He, H.P., Li, T., Tao, Q., Chen, T.H., Zhang, D., Zhu, J.X., Yuan, P., and Zhu, R.L. (2014) Aluminum ion occupancy in the structure of synthetic saponites: Effect on crystallinity. American Mineralogist, 99, 109–116.
Kossel, W. (1927) Zur theorie des kristallwachstums. Nachrichten von der Gesellschaft der Wissenschaften zu Göttingen, Mathematisch-Physikalische Klasse, 1927, 135–143.
Lee Penn, R., Tanaka, K., and Erbs, J. (2007) Size dependent kinetics of oriented aggregation. Journal of Crystal Growth, 309, 97–102.
Lee, G.S., Lee, Y.-J., and Yoon, K.B. (2001) Layer-by-layer assembly of zeolite crystals on glass with polyelectrolytes as ionic linkers. Journal of the American Chemical Society, 123, 9769–9779.
Lee, J., Yang, J., Kwon, S.G., and Hyeon, T. (2016) Nonclassical nucleation and growth of inorganic nanoparticles. Nature Reviews Materials, 1, 1–16.

Li, M., Schnablegger, H., and Mann, S. (1999) Coupled synthesis and self-assembly of nanoparticles to give structures with controlled organization. Nature, 402, 393–395.

Liu, L., Park, J., Siegel, D.A., McCarty, K.F., Clark, K.W., Deng, W., Basile, L., Idrobo, J.C., Li, A.-P., and Gu, G. (2014) Heteroepitaxial growth of two-dimensional hexagonal boron nitride templated by graphene edges. Science, 343, 163–167.

Lupulescu, A.I., and Rimer, J.D. (2014) In situ imaging of silicalite-1 surface growth reveals the mechanism of crystallization. Science, 344, 729–732.

Nanev, C.N. (2015) 7—Theory of nucleation. In T. Nishinaga, Ed., Handbook of Crystal Growth, 2nd ed., p. 315–358. Elsevier.

Oaki, Y., and Imai, H. (2005) The hierarchical architecture of nacre and its mimetic material. Angewandte Chemie International Edition, 44, 6571–6575.

Penn, R.L., and Banfield, J.F. (1998a) Imperfect oriented attachment: Dislocation generation in defect-free nanocrystals. Science, 281, 969–971.

——— (1998b) Oriented attachment and growth, twinning, polytypism, and formation of metastable phases: Insights from nanocrystalline TiO_2. American Mineralogist, 83, 1077–1082.

——— (1999) Morphology development and crystal growth in nanocrystalline aggregates under hydrothermal conditions: Insights from titania. Geochimica et Cosmochimica Acta, 63, 1549–1557.

Ross, M., Takeda, H., and Wones, D.L. (1966) Mica polytypes: systematic description and identification. Science, 151, 191–193.

Smeets, P.J.M., Finney, A.R., Habraken, W.J.E.M., Nudelman, F., Friedrich, H., Laven, J., De Yoreo, J.J., Rodger, P.M., and Sommerdijk, N.A.J.M. (2017) A classical view on nonclassical nucleation. Proceedings of the National Academy of Sciences, 114, E7882–E7890.

Smith, J.V., and Yoder, H.S. (1956) Experimental and theoretical studies of the mica polymorphs. Mineralogical Magazine and Journal of the Mineralogical Society, 31, 209–235.

Stranski, I.N. (1928) Zur theorie des kristallwachstums. Zeitschrift für Physikalische Chemie, 136, 259–278.

Sunagawa, I. (2007) Crystals: Growth, morphology, and perfection, 308 p. Cambridge University Press.

Sunagawa, I., and Koshino, Y. (1975) Growth spirals on kaolin group minerals. American Mineralogist, 60, 407–412.

Tan, W., He, H.P., Wang, C.Y., Dong, H., Liang, X.L., and Zhu, J.X. (2016) Magnetite exsolution in ilmenite from the Fe-Ti oxide gabbro in the Xinjie intrusion (SW China) and sources of unusually strong remnant magnetization. American Mineralogist, 101, 2759–2767.

ten Wolde, P.R., and Frenkel, D. (1997) Enhancement of protein crystal nucleation by critical density fluctuations. Science, 277, 1975–1978.

Wallace, A.F., Hedges, L.O., Fernandez-Martinez, A., Raiteri, P., Gale, J.D., Waychunas, G.A., Whitelam, S., Banfield, J.F., and De Yoreo, J.J. (2013) Microscopic evidence for liquid-liquid separation in supersaturated $CaCO_3$ solutions. Science, 341, 885–889.

White, G.N., and Zelazny, L.W. (1988) Analysis and implications of the edge structure of dioctahedral phyllosilicates. Clays and Clay Minerals, 36, 141–146.

Yang, Z.Y., Wang, R.C., Che, X.D., Yin, R., Xie, L., and Hu, H. (2020) Formation of columbite and microlite after alteration of Nb- and Ta-bearing biotite from the Lizaizhai pegmatite (Guangning ore district Guangdong, South China): Identification of a new potential Nb-Ta mineralization type. Journal of Asian Earth Sciences, 190, 104154.

Zhang, H., De Yoreo, J.J., and Banfield, J.F. (2014) A unified description of attachment-based crystal growth. ACS Nano, 8, 6526–6530.

Endnote:

[1]Deposit item AM-21-67529, Supplemental Material. Deposit items are free to all readers and found on the MSA website, via the specific issue's Table of Contents (go to http://www.minsocam.org/MSA/AmMin/TOC/2021/Jun2021_data/Jun2021_data.html).